ARCHIVE OF MECHANICAL ENGINEERING

DOI: 10.24425/ame.2025.155870 2025, Vol. 72, No. 4, pp. 607–626

Maciej ROSZAK [1], Dariusz PYKA [1], Maksymilian STĘPCZAK [1], Paweł SWEKLEJ [2], Krzysztof JAMROZIAK [1], Mirosław BOCIAN [1]

Ballistic resistance tests of a fuel tank intended for installation in an armored vehicle

Received 24 April 2025, **Revised** 10 September 2025, **Accepted** 16 September 2025, **Published online** 20 November 2025

Keywords: impact loads, ballistic resistance, fuel tank, Finite Element Method

Fuel tanks in vehicles traveling in danger zones are susceptible to damage resulting from shelling. Ensuring adequate strength of this type of construction elements is extremely important. The object of the research was a fuel tank from a leading manufacturer, declared as made of an external coating that allows for closing gunshot holes. The tank was subjected to fire in two variants: without additional protection and with additional protection in the form of Armox 500T armor plate with a thickness of 4.5 mm. Additionally, the authors also performed numerical analyzes in the Abaqus/-Explicit program, which were used to reproduce the physical phenomena occurring during shooting. The developed geometric models and the declared initial boundary conditions reflected the actual test conditions, and the Johnson-Cook model and the failure model were used. These tests assessed the tank's resistance to shooting, the extent to which the gunshot holes closed and the possibility of fuel ignition inside the tank. Then, verification tests were carried out in which 4 mm sheet metal panels were shot at to validate the numerical results for the adopted material model of the shield. The obtained results from numerical simulations corresponded appropriately with the results of experiments. Building upon this correspondence, the study offers an innovative contribution by integrating a comprehensive ballistic evaluation of a real, self-sealing fuel tank system with detailed numerical validation based on advanced material failure modelling and parameter sensitivity analysis. The results obtained may serve as a reference for the design and optimization of protective systems in armored vehicles, particularly regarding enhancing fuel system survivability under ballistic impact.

✉ Maciej ROSZAK, email: maciej.roszak@pwr.edu.pl

[1]Department of Mechanics, Materials and Biomedical Engineering, Wrocław University of Science and Technology, Wrocław, Poland

[2]Military Institute of Armament Technology, Zielonka, Poland

1. Introduction

Fuel tanks are among the most vulnerable components in vehicles operating in armed conflict zones or during VIP transport missions [1, 2].

Shooting through a tank during an attack on a vehicle may have many negative consequences. Weakening the structure by shooting through the tank may lead to:

- rapid loss of fuel and thus immobilization of the vehicle;
- leakage of the fuel mixture, resulting in ignition and explosion;
- due to the pressure exerted and the weakening of the structure, the complete collapse of the tank.

Therefore, it is extremely important to properly secure this element of the structure, as it directly affects the safety of the traveling crew and vehicle users. For this purpose, various structures using light materials are used [3].

Modern military vehicles, in particular high-mobility armored vehicles intended for patrol and convoy missions, are a key element of modern armed forces. Their structure, based on advanced materials and technologies, is designed to withstand threats such as machine gun fire or explosions of improvised explosive devices (IEDs). The key determinants of these technologies are Mine Resistant Ambush Protected (MRAP) and MRAP All Terrain Vehicle (M-ATV) class vehicles, such as RG-31/32, Cougar, Dingo 2, Zubr/Tur or Armored Multi-Role Vehicle (AMRV G10). These structures have been the subject of numerous studies including design processes, ballistic tests and analyses of crew comfort and body functionality [4, 5]. The primary purpose of designing such vehicles is to protect the crew and critical systems, including fuel tanks, which, if damaged, can lead to catastrophic consequences. Research on protective materials focuses on creating multi-layer composite structures [6–9]. An example is the "Composite Armor Philosophy" (CAP) design philosophy proposed by Tsirogiannis and co-authors, which integrates various materials such as ceramics, steel, and polymer composites to maximize resistance to ballistic threats [10]. The use of such solutions significantly reduces the weight of the structure, which increases the mobility of the vehicle while maintaining high standards of protection.

Materials used in armor construction, such as Armox 500T (A500T), are intensively researched for their mechanical properties and behavior during high-velocity impacts. Iqbal et al.'s research on A500T steel showed that its high tensile strength and resistance to dynamic deformation make this material suitable for use in armored vehicles [11]. Similar studies on the behavior of composites under high bullet velocities confirm their effectiveness in reducing penetration and dissipating impact energy [12–16].

Protecting fuel tanks in armored vehicles is one of the most important challenges in the design of these structures. Shooting through the fuel tank may lead to vehicle immobilization, fuel leakage and ignition, or even explosion. Ren and co-authors conducted combined experimental and numerical studies on the penetration effects of liquid-filled tanks, pointing out the importance of internal pressure

damping in minimizing damage [17]. Similar research by Liu and co-authors on tanks with rubber shock-absorbing layers highlighted the importance of multi-layer materials in reducing tank deformation under bullet impacts [18, 19]. Numerical modeling plays a key role in assessing the behavior of armored structures. Simulations conducted by Spear and co-authors indicate that modeling at high strain rates allows accurate prediction of the behavior of materials under dynamic loads [20]. The Johnson-Cook (J-C) model, used to simulate deformation and failure, is one of the most frequently used tools in fuel tank analyses [21–26].

Although previous studies have examined the ballistic performance of protective materials and fluid-filled containers, few have addressed the behavior of complete, commercially available fuel tank systems under real ballistic conditions. This work fills that gap by evaluating a self-sealing SAFETANK from Hutchinson®, both in its base configuration and with added Armox 500T steel protection. The experimental tests, conducted with multiple calibers and verified via high-speed imaging, offer a rare, system-level insight into ballistic resistance. Moreover, the study integrates detailed finite element modelling using the Johnson-Cook constitutive and failure models, with parameter sensitivity analysis, including displacement at failure and stress erosion. These numerical results were validated against experimental observations of penetration, deformation, and crater geometry.

2. Object of research

The subject of the research was a fuel tank made by HUTCHINSON® under the name SAFETANK series Nbr. 120710-04. This tank is intended for military use. Due to its advantages in ballistic protection, it is installed in armored vehicles. According to HUTCHINSON®, the fuel tank supplied for ballistic testing is a safe fuel tank classified by the manufacturer as Safetank. According to advertising materials [27], it is made of an external coating that closes holes caused by small ammunition and shrapnel fire and stops fuel leaks. This way it is possible to reduce:

- risk of fire and explosion;
- crew injuries from external fires;
- ignition of fuel vapors during explosion and penetration by ammunition.

The protective coating defined by the manufacturer as the Safetank has the following advantages:

- eliminates the need for additional armor with metal or composite plates;
- has a positive effect on the materials used in the construction of the tank: plastic or aluminum;
- can reduce the system weight to approximately 100 kg in some applications.

The tank that was analyzed is a cuboid with dimensions of 610×610×450 mm, its view is shown in Fig. 1. An example of the use of the fuel tank is shown below Fig. 2.

Fig. 1. General view of the tank with the manufacturer's plate

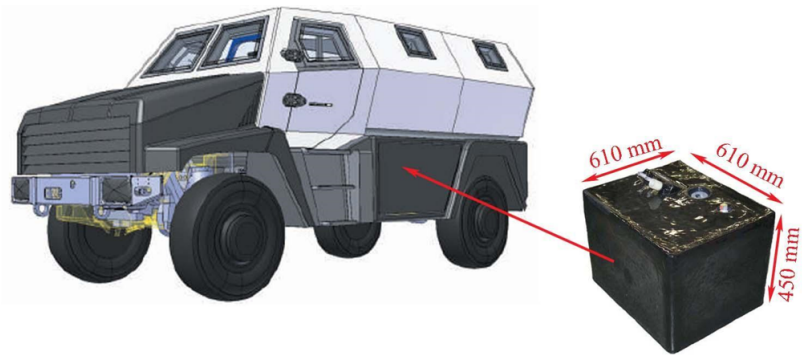

Fig. 2. General view of the Safetank fuel tank with optional location in the vehicle AMRV G10 – 3D model

3. Research station

Shooting was carried from a distance of 3 m for pistol ammunition, and for the remaining ammunition the shooting distance was 10 m. Each time, the velocity of the fired bullet was measured using a measuring device that gave the average value measured between the starting and ending gates. Measurements that significantly deviated from the values specified in the PN EN 1522 standard were rejected [28]. The diagram of the test stand is shown below Fig. 3. Before starting the tests, the fuel tank was enclosed with a structure which, on the one hand, provided hooks for mounting the target under fire, and on the other hand, this structure was used to enclose the fuel tank with additional covers. The method of housing the tank is shown in Fig. 4.

Three types of ammunition were used for firing, the parameters of which are summarized in the table below (Table 1).

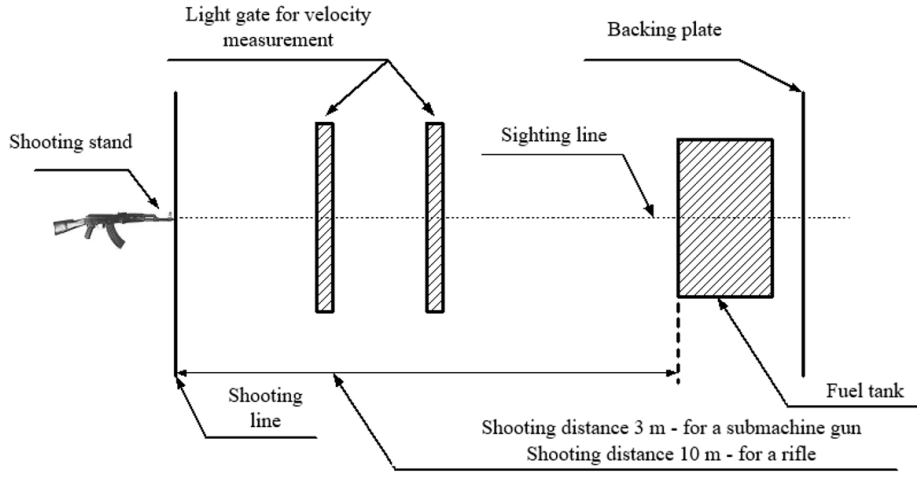

Fig. 3. Ballistic test diagram

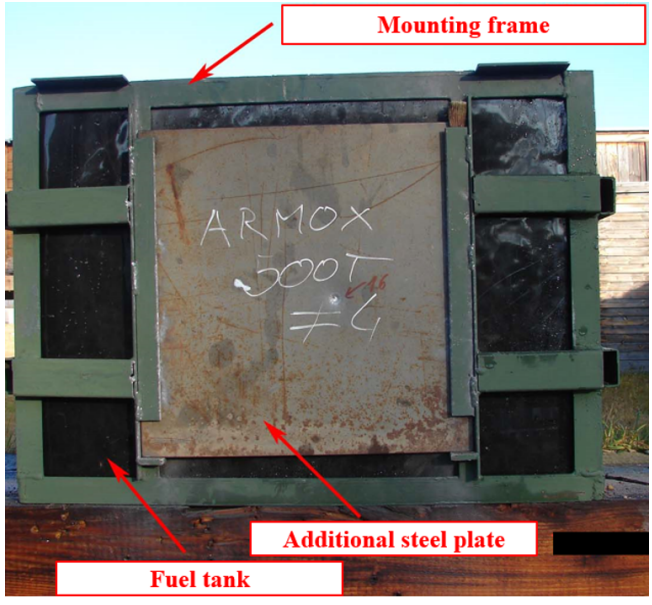

Fig. 4. Tested object at a military training ground

Table 1. Parameters of the ammunition used

Ammunition	Round mass [g]	Projectile mass [g]	Initial velocity [m/s]	Kinetic energy [J]
9 × 19 mm FMJ PARA	12.0	8.0	356	518
7.62 × 39 mm FMJ PS	16.2	7.9	720	2070
.308 WIN Match	25.1	10.9	780	3316

4. Preparation of numerical model

The (J-C) constitutive equation (1) is suitable for computational purposes due to its simplicity and the use of parameters that are relatively easy to determine. It is commonly used in CAE programs, such as ABAQUS, LS-Dyna [29–31].

$$\sigma_y = \left(A + B\bar{\varepsilon}^{p^n}\right)\left(1 + C\ln\dot{\varepsilon}^*\right)\left(1 - T^{*m}\right), \tag{1}$$

where ε is the plastic strain, $\dot{\varepsilon}$ – the plastic strain rate, A, B, C, n and m – the J-C material behavior coefficients where A is the yield stress of the material under reference conditions, B is the strain hardening constant, C is the strengthening coefficient of the strain rate, n is the strain hardening coefficient and m is the thermal softening exponent.

Material failure equations regulate material strength and/or material stiffness as a function of the damage variable. When the damage variable reaches a critical value, damage propagates (crack). In this relationship, the deformation occurring at the moment of destruction is described by the relationship (2).

$$\varepsilon_f = \left[D_1 + D_2 e^{D_3\sigma^*}\right]\left[1 + D_4\ln\dot{\varepsilon}^*\right]\left[1 + D_5 T^*\right], \tag{2}$$

where ε_f – the plastic strain to fracture; σ^* – the equivalent stress, D_1, D_2, D_3, D_4 and D_5 – the input constants determined empirically.

Geometric models were developed based on the actual structure of the projectiles (Fig. 5) and tank (Fig. 6). The projectiles were discretized with a grid of hex elements, dimensions 0.1 to 0.5 mm from Abaqus/Explicit library. The front wall of the tank was mapped, the dimensions of the finite elements were from 0.5 mm at the point of compaction (projectile impact) to 10 mm at the outer edges. In the subsequent model validation for the 4 mm sheet impact, elements with a size of 0.2 mm were used at the projectile impact point. In the case of the sheet metal, the side edges were fixed as in the mounting frame, while in the case of the tank wall the side surfaces were constrained to prevent displacement in all directions (U1 = UR1 = U2 = UR2 = U3 = UR3 = 0, where U – displacements; UR – rotations), simulating fixed boundary conditions in the frame.

To describe the behavior of materials, the (J-C) constitutive model was used together with the failure model in which the term responsible for thermal softening was omitted. During the simulation, the displacement at failure parameter –

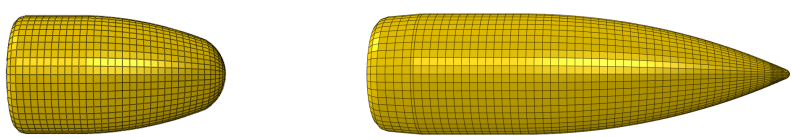

(a) (b)

Fig. 5. Examples of numerical models of projectiles discretized with 0.5 mm hex mesh: (a) 9 × 19 mm FMJ PARA projectile, (b) 7.62 × 39 mm FMJ PS projectile Kalashnikov

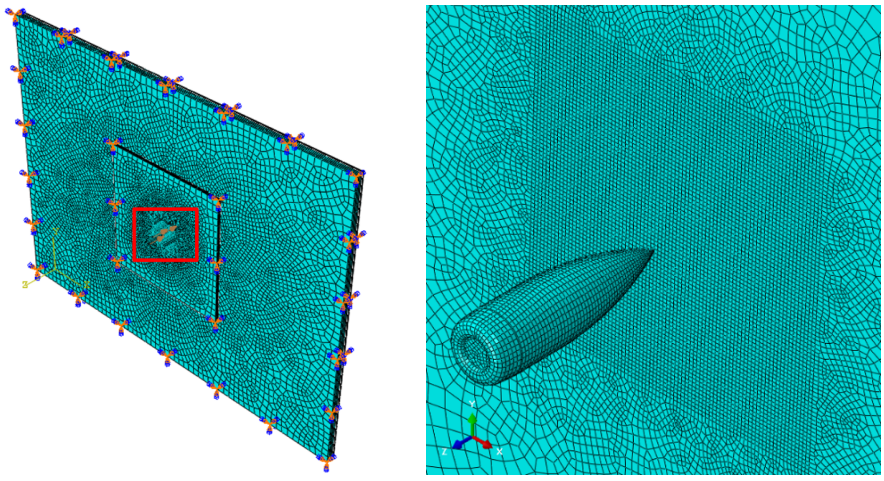

(a) (b)

Fig. 6. Numerical model of the projectile-tank wall: (a) general view; (b) close-up of the mesh densification area (0.5 mm hex elements)

a parameter describing the nature of material degradation in the Abaqus/Explicit software was modified. When the failure criterion is met, the element is not immediately removed, but its stiffness is gradually degraded and secured by a given stabilizing criterion, i.e., critical stress, so that no element is subject to excessive deformation. The material parameters are listed in the tables below (Table 2 and 3).

Table 2. Material parameters in the (J-C) strength model [11, 20, 29, 32, 33]

Projectile material	E [GPa]	v [–]	A [MPa]	B [MPa]	n [–]	c [–]
Lead (core) [29]	13.00	0.42	35	46	0.48	0.0100
Brass (jacket) [29]	130.00	0.38	112	505	0.42	0.0100
7.62 × 39 mm steel core (C45 steel) [33]	210.00	0.33	553	600	0.36	0.0134
A500T (additional protection) [11]	201.00	0.33	1372	835	0.25	0.0620
Elastomer (outer fuel tank's layer) [32]	1.57	0.49	1 0	9500	1.32	–
Aluminum (internal fuel tank's layer) [20]	70.00	0.30	324	113	0.42	0.0020

Table 3. Material parameters in the (J-C) failure model [11, 20, 34, 35]

Material	D_1 [–]	D_2 [–]	D_3 [–]	D_4 [–]	Displacement at failure [mm]/ critical stress [MPa]
A500T (additional protection) [11]	0.0429	2.1521	–2.7575	–0.0066	0.35 / 3700
Aluminum (internal fuel tank's layer) [20, 34, 35]	–0.7700	1.450	–0.470	0	0

The critical stress model was used to describe the discontinuity of the elastomeric material, which led to material failure upon reaching a critical stress value. The tensile strength value was obtained in the authors' previous studies [32].

5. Results of ballistic tests

Based on a preliminary visual inspection after firing the fuel tank with ballistic shields, the behavior of the Safetank shell to direct fire with small arms projectiles was checked. The results of the ballistic tests using tested ammunition are shown in Table 4.

Table 4. Initial boundary conditions of projectiles during field tests

No.	No. of shot	Type of ammunition	Distance [m]	Initial velocity [m/s]	Initial energy [J]	Effect
1	31	9 × 19 mm Parabellum FMJ (WA)	3	–	–	P
2	32			–	–	P
3	33			–	–	P
4	28	7.62 × 39 mm FMJ PS (WA)	10	704	1957.7	P
5	29			701	1941.0	P
6	30			695	1907.9	P
7	16	7.62 × 39 mm FMJ PS (A)		702	1946.6	B
8	17			698	1924.5	B
9	18			–	–	B
10	19	.308 WIN Match (A)		763	3172.8	P
11	20			771	3239.7	P
12	21			772	3248.1	P

where B – no penetration/incomplete penetration, P – full penetration, WA – Without Armor, A – Armored

First, the fuel tank was fired 7.62 × 39 mm FMJ PS projectile Kalashnikov and 9 mm FMJ Parabellum projectile. The results of this firing are illustrated in Figs. 7 and 8. In both cases, the tank was shot through, but its protective coating caused the damaged wall to heal and the leaks quickly stopped.

Secondly, tanks shielded with A500T metal plate were tested. Based on the results obtained (Fig. 9), it was concluded that the firing test with a 7.62 × 39 mm FMJ PS projectile Kalashnikov ended negatively. This caliber failed to penetrate the tank armor, suggesting its effectiveness against this type of ammunition.

A shooting test with a .308 WIN Match bullet was successful (Fig. 10). The bullet passed through the shell of the tank, causing a characteristic leakage of liquid medium (Fig. 11). Nevertheless, the material properties of the tank allowed the perforation to quickly seal itself, significantly reducing further fluid loss.

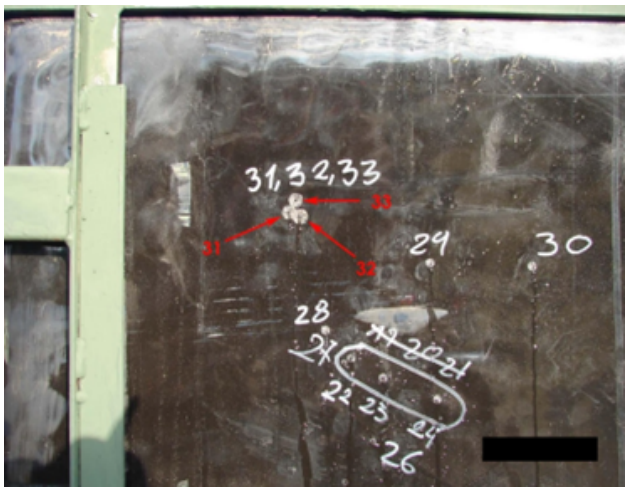

Fig. 7. Fuel tank fired with a 9 × 19 mm FMJ Parabellum projectile – shots 31–33

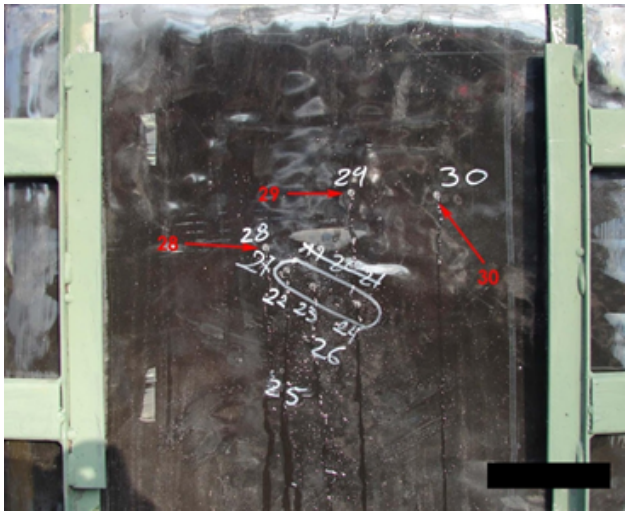

Fig. 8. Fuel tank fired by a 7.62 × 39 mm FMJ PS projectile Kalashnikov – shots 28–30

The fuel tank underwent ballistic testing with various calibers, including 7.62× 39 mm FMJ PS bullets Kalashnikov and 9 mm FMJ Parabellum pistol bullets, as well as .308 WIN Match bullets. Initial tests with unshielded tanks revealed that, while the bullets penetrated the tank walls, the protective coating facilitated rapid self-sealing of the perforations, effectively halting leaks. Further tests with tanks shielded by A500T metal plates demonstrated the armor's effectiveness, as the 7.62 × 39 mm FMJ PS bullets failed to penetrate. However, the .308 WIN Match

Fig. 9. Fuel tank covered with A500T fired with a 7.62 × 39 mm FMJ PS projectile Kalashnikov – shots 16–18

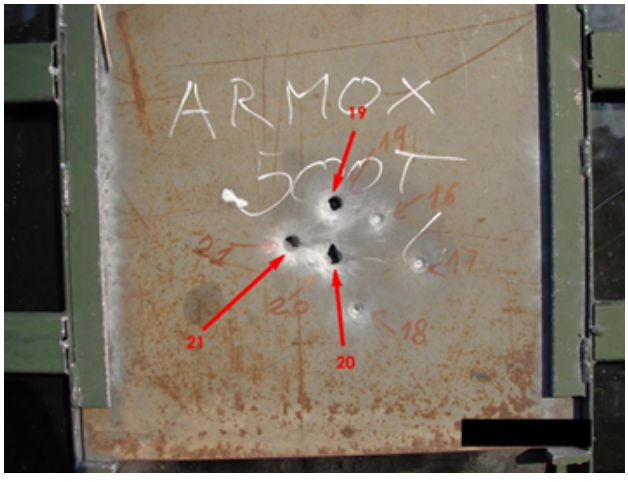

Fig. 10. Fuel tank covered with A500T tested with .308 WIN Match bullet – shots 19–21

bullet successfully breached the tank, causing leakage, which was again mitigated by the tank's self-sealing material properties, significantly reducing fluid loss. When unprotected, the tank was penetrated by all types of ammunition tested. However, the self-sealing material reduced leakage after impact (Fig. 7 and 8). With the addition of a 4.5 mm A500T plate, the tank resisted 7.62 × 39 mm FMJ PS bullets (Fig. 9), but the .308 WIN Match bullet still caused full perforation (Fig. 10 and 11). This confirmed that while the armor improved resistance, it was not sufficient against all threats.

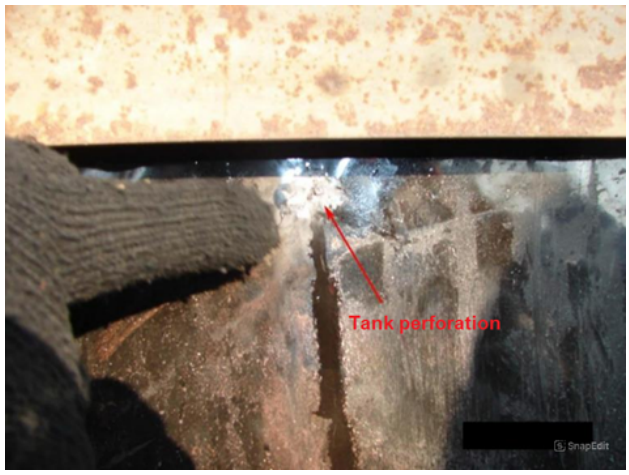

Fig. 11. Fuel tank shot through with .308 WIN Match bullet – shot 20, with characteristic leakage of tank contents

6. Results of numerical analysis

The final stage of the research was to verify the correspondence between the numerical research results and the field test results. The verification was carried out in terms of observing the final effect of the fire, i.e., penetration or lack of penetration of the material system of the shield. First, the penetrating capabilities of the 9 × 19 mm FMJ Parabellum bullet were checked. The simulation results are shown below for the system with an additional steel sheet (Fig. 12) and without an additional cover (Fig. 13). As in the case of the experiment, a breakthrough was obtained for the tank without additional cover.

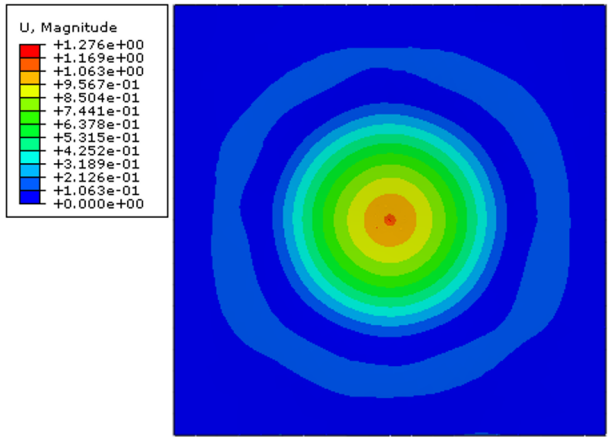

Fig. 12. Additional steel cover – complete stopping of the 9 × 19 mm FMJ PARA projectile – deflection of the steel plate [mm]

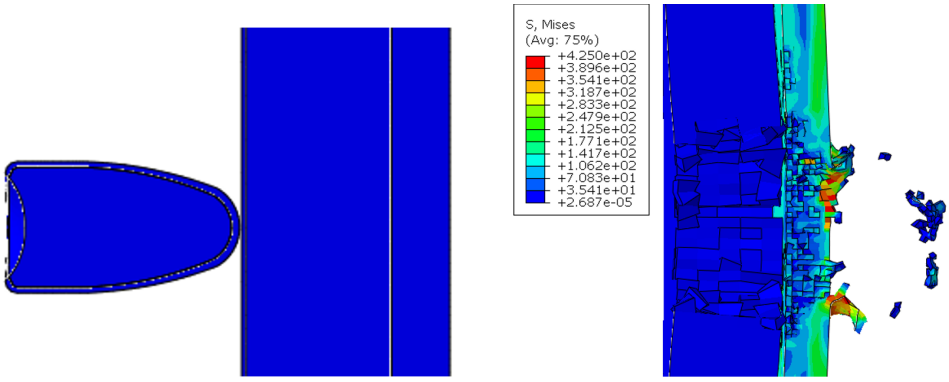

(a) (b)

Fig. 13. Complete penetration of the tank wall without additional protection with the 9×19 mm FMJ PARA projectile – Huber-Mises-Hencky stress [MPa]: (a) initial position; (b) after 1×10^{-4} s

The same results were also obtained in the simulation results of the impact of the 7.62×39 mm FMJ PS bullet. The use of an additional shield allowed the projectile to be completely stopped (Fig. 14), but the outer layer of the shield was damaged, as in Fig. 9. Complete penetration was achieved for the material system of the samples without additional protection in the form of a steel shield (Fig. 15).

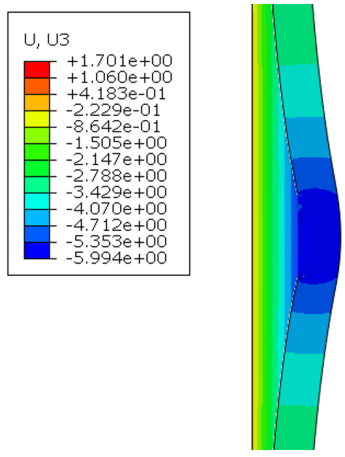

Fig. 14. Additional steel cover – complete stopping of the 7.62×39 mm FMJ PS projectile – deflection of the steel plate [mm]

The only bullet capable of penetrating the tank's material system with additional protection was the .308 WIN bullet. As in the case of experimental tests, complete penetration of the tank wall was achieved along with an additional cover (Fig. 16).

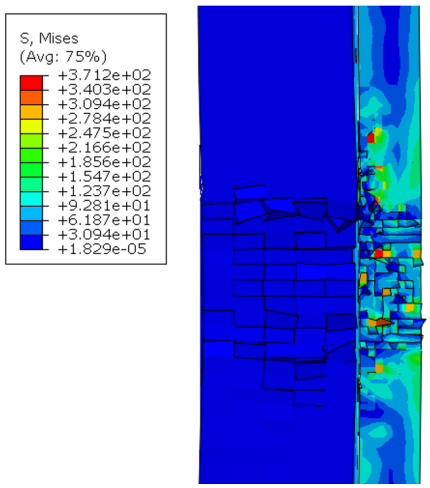

Fig. 15. Complete penetration of the tank wall without additional protection by the 7.62 × 39 mm FMJ PS projectile – Huber-Mises-Hencky stress [MPa]

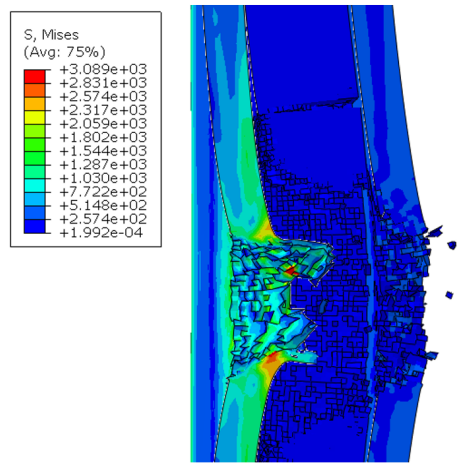

Fig. 16. Complete penetration of the sheet metal and tank wall by a .308 WIN projectile – Huber-Mises-Hencky stress [MPa]

To summarize the conducted numerical studies, they correspond in terms of comparing the effect of shooting with experimental studies. Convergence in this respect was achieved. However, in the future, more advanced methods should also be used to verify the correspondence of numerical models with the experiment, e.g., in the form of X-ray cameras to analyze the velocity of the projectile after penetrating the shield.

7. Validation of obtained results

As a result of the research, a correlation was obtained between the results of experimental and numerical research (Table 5).

Table 5. Summary of research results

Ammunition	Experiment	Simulation
With additional shield		
9 × 19 mm FMJ PARA	B	B
7.62 × 39 mm FMJ PS	B	B
.308 WIN Match	P	P
Without additional shield		
9 × 19 mm FMJ PARA	P	P
7.62 × 39 mm FMJ PS	P	P
.308 WIN Match	P	P

where B – no penetration/incomplete penetration, P – full penetration.

Verification of the numerical analysis was carried out using the results of ballistic tests on a 4 mm thick A500T sheet. The moment of impact of the bullet was captured using PHANTOM VEO 710L and TMX high-speed cameras. Both the lack of penetration of the 7.62×39 mm FMJ bullet (Fig. 17) and the penetration achieved by the .308 WIN Match bullet were captured, confirming the result of the numerical simulation (Fig. 18).

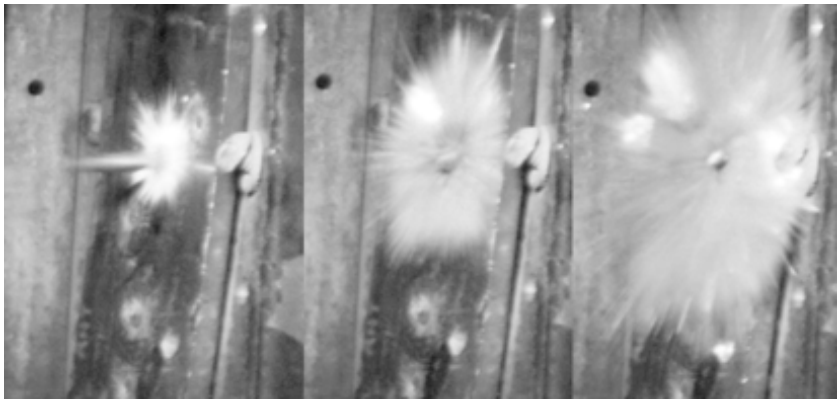

Fig. 17. 7.62 × 39 mm FMJ PS bullet stopped by an armored plate

Fig. 18. Plate penetration by the .308 WIN Match bullet

Analysis of the recorded frames 3, 5, and 9 made it possible to determine the displacement of the projectile relative to the edge of the plate after perforating the A500T steel sample. Based on this, the residual velocity of the projectile was determined to be 566 m/s.

An additional example comparison of the values obtained from simulation and experiment is shown below for the most representative case (Fig. 19). For comparison purposes, the values of the crater diameter and sample deflection are listed in the table below (Table 6).

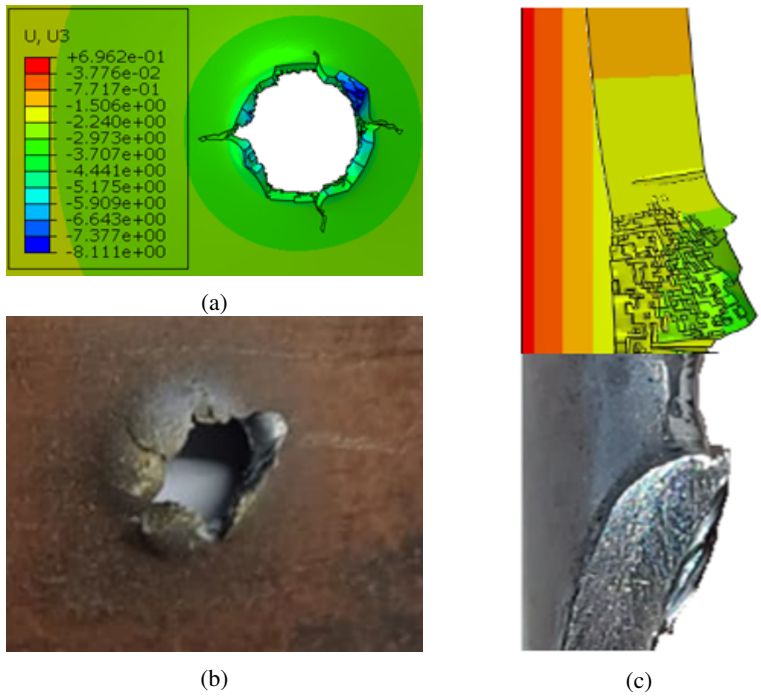

Fig. 19. Results of validation of ballistic test: (a) numerical simulation (units in mm); (b) experiment; (c) example cross-section comparison

Table 6. Comparison of obtained results for ballistic test and numerical simulations

Variant	Experiment	Simulation	Error
7.62 × 39 mm projectile – hole diameter	–	–	–
7.62 × 39 mm projectile – deflection	6.63 ± 0.01 mm	5.99 mm	9.7%
.308 WIN projectile – hole diameter	8.68 ± 0.40 mm	8.91 mm	2.6%
.308 WIN – deflection	11.09 ± 0.67 mm	12.11 mm	9.2%

A comparison of the results for different values of the failure criterion displacement at failure is also presented below (Fig. 20). This illustrates the differences that occur depending on the applied displacement-to-failure value. By introducing an

additional erosion criterion, where the stress limit was set to 3700 MPa, it was possible to reduce the occurrence of excessively deformed finite elements. Noticeable differences can be observed in the obtained values compared to the most reliable case (Fig. 19), which used a stress limit of 3700 MPa and a displacement at failure of 0.35 mm. These differences are evident not only in the visual aspects of the results, such as the shape of the craters, but also in the crater deflection (Fig. 20) and the residual velocity of the projectile after perforation, as shown in the graph below (Fig. 21). Also, the influence of stress value was also analyzed.

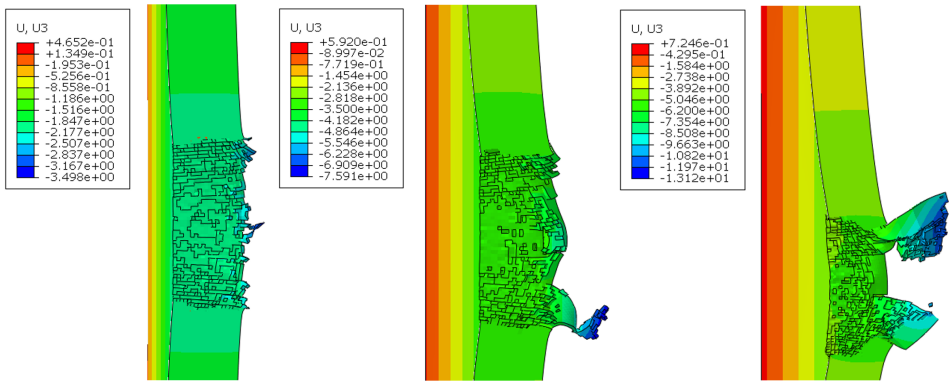

(a) (b) (c)

Fig. 20. Obtained results for 3700 MPa erosion and different values of displacement of failure: (a) 0 mm displacement; (b) 0.2 mm displacement; (c) 1 mm displacement. Units in (mm)

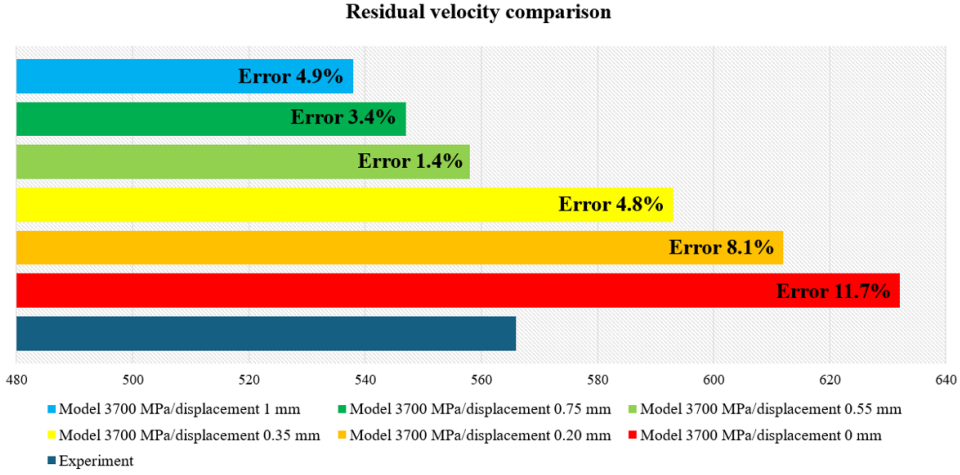

Fig. 21. Comparison of residual velocity and different variants of displacement of failure

The numerical results for the .308 WIN projectile penetration were in close agreement with the experimental data, with discrepancies in deformation param-

eters and crater diameter remaining below 10%, thereby confirming the accuracy of the model and the adopted failure criteria. Simulation variants incorporating different displacement-at-failure values demonstrated a significant influence of this parameter on the predicted residual velocity, both excessively low and excessively high values led to considerable deviations from the experimental results.

The findings indicate that, for an effective assessment of ballistic protection, particularly in the context of high-energy threats, it is essential to consider not only the occurrence of penetration but also the actual residual velocity of the projectile, as this determines the potential for impacting components located behind the armor.

Variations in the value of critical stress for erosion were also found to have a substantial effect. At both higher and lower critical stress values, discrepancies frequently exceeded 20–30%. For excessively low erosion thresholds, elements failed prematurely, resulting in overestimated projectile velocities. Conversely, overly high values led to excessive and unrealistic plate deflection.

8. Conclusions

On this basis, the following conclusions were made:

1. The ballistic resistance achieved by the SAFETANK system equipped with a 4.5 mm A500T steel plate demonstrates protection levels comparable to those reported for more complex multilayer armor systems based on ceramics or polymer composites [10, 11].
2. Penetration by any type of ammunition, and the contents of the tank spill out.
3. Additional protection in the form of A500T armored steel allows the solution to maintain the assumed bullet resistance, providing protection against 9×19 mm FMJ PARA and 7.62×39 mm FMJ PS projectiles.
4. The solution used does not provide protection against the .308 Winchester bullet.
5. Despite being shot through, the rubber material used in the tank allows the firing site to be sealed, thanks to which the leakage of the contents is quickly limited, in accordance with the manufacturer's declarations.
6. Correspondence of the results in terms of penetration/no penetration was obtained, also in case of samples' deflection, but the methods used would require further experimental verification using, for example, X-ray cameras.
7. Additional studies were carried out to verify the accuracy of numerical model by comparing the residual velocity values after perforation. The multi-stage verification of the model made it possible to identify the most representative case, which provided the highest consistency in terms of visual appearance, crater dimensions and satisfactory residual velocity values. The applied and properly calibrated damage model is crucial in the context of obtained numerical simulations results.

8. Furthermore, the numerical simulations carried out using the Johnson-Cook constitutive and failure models showed very good agreement with the experimental data. The differences in crater diameter and deflection between simulations and tests remained below 10%, which aligns well with, or improves upon, results reported in related literature [20, 22, 30]. The implemented sensitivity analysis of failure parameters further enhanced the reliability of the model. This reinforces the applicability of the adopted modelling methodology for predicting the behavior of composite and armored structures under ballistic impact.

References

[1] NATO AEP-55 STANAG 4569:2020. *Procedures for evaluating the protection levels of logistic and light armoured vehicles for KE and artillery threat*.

[2] E. Risberg. *A Pre-Study on Implementing Self-Sealing Techniques in the Fuel Tank of the Combat Vehicle 90*. BAE Systems Hägglunds, 78, 2014.

[3] A. Purbey, R. Selvaray, and M. Ramamoorthy. Impact response of a partially filled fuel tank subjected to high-velocity projectiles. *Australian Journal of Mechanical Engineering*, 22(2):342–360, 2024. doi: 10.1080/14484846.2022.2094536.

[4] B.B. Singh, G. Sukumar, P. Senthil, P.K. Jena, P.R. Reddy, K.S. Kumar, V. Madhu, and G.M. Reddy. Future armour materials and technologies for combat platforms. *Defence Science Journal*, 67:412–419, 2017. doi: 10.14429/dsj.67.11468.

[5] O. Sapunkov. Historical trends and parameter relationships in the design of armored fighting vehicles. *SAE Technical Paper 2024-01-3837*, 2024. doi: 10.4271/2024-01-3837.

[6] H. Lee, J. Choi, G. Kim, and K. Shin. A study on the armor optimization of military vehicle. *Journal of the Korea Institute of Military Science and Technology*, 16:405–413, 2013. doi: 10.9766/kimst.2013.16.4.405. (in Chinese).

[7] J. Kwon, G. Kim, Y. Cho, and K. Won. Technological trends in wheeled armoured vehicle from patent analysis. *Journal of Advances in Military Studies*, 6(2):91–114, 2023. doi: 10.37944/jams.v6i2.193.

[8] H. Kim. Construction of protection system for next generation tanks. *Korean Journal of Military Affairs*, 11:157–180, 2022. doi: 10.33528/kjma.2022.6.11.157. (in Korean).

[9] P. Hazell. *Armour: Materials, Theory, and Design*. CRC Press, 2015. doi: 10.1201/b18683.

[10] E.C. Tsirogiannis, F. Psarommatis, A. Prospathopoulos, and G. Savaidis. Composite armor philosophy (CAP): Holistic design methodology of multi-layered composite protection systems for armored vehicles. *Defence Technology*, 41:181–197, 2024. doi: 10.1016/j.dt.2024.07.009.

[11] M.A. Iqbal, K. Senthil, P. Sharma, and N.K. Gupta. An investigation of the constitutive behavior of Armox 500T steel and armor piercing incendiary projectile material. *International Journal of Impact Engineering*, 96:146–164, 2016. doi: 10.1016/j.ijimpeng.2016.05.017.

[12] B. Bakri, M.S. Fadly, K. Anwar, S. Chandrabakty, Mustafa, Naharuddin, and Fauzan. Numerical research on the impacts of composite panel ballistic using perforated plate for combat vehicle. *Proceedings of the 4th International Seminar on Science and Technology (ISST 2022)*, 2023. doi: 10.2991/978-94-6463-228-6_3.

[13] C.F. Yen. Ballistic impact modeling of composite materials. *7th International LS-DYNA Users Conference*, 2002.

[14] W. Cao and Y. Yao. Application trend of nonmetallic materials in the construction and development of armored equipment. *2020 International Conference on Social and Human Sciences (ICSHS2020)*, pages 286–289, 2020. doi: 10.38007/proceedings.0000052.

[15] S. Siengchin. A review on lightweight materials for defence applications: A present and future developments. *Defence Technology*, 24:1–17, 2023. doi: 10.1016/j.dt.2023.02.025.

[16] Y. Bao, X. Gao, Y. Wu, M. Sun, and G. Li. Research progress of armor protection materials. *Journal of Physics: Conference Series*, 1855:012035, 2021, doi: 10.1088/1742-6596/1855/1/012035.

[17] P. Ren, L. Shi, R. Ye, D. Chai, W. Zhao, J. Wu, W. Zhang, and Z. Mu. A combined experimental and numerical investigation on projectiles penetrating into water-filled container. *Thin-Walled Structures*, 143:106230, 2019. doi: 10.1016/j.tws.2019.106230.

[18] F. Liu, X. Kong, C. Zheng, S. Xu, W. Wu, and P. Chen. The influence of rubber layer on the response of fluid-filled container due to high-velocity impact. *Composite Structures*, 183:671–681, 2018. doi: 10.1016/j.compstruct.2017.09.005.

[19] P. Zhang, X. Kong, Z. Wang, C. Zheng, H. Liu, G. Shi, J. Dear, and W. Wu. High velocity projectile impact of a composite rubber/aluminium fluid-filled container. *International Journal of Lightweight Materials and Manufacture*, 4(1):1–8,2020. doi: 10.1016/j.ijlmm.2020.06.007.

[20] D.G. Spear, A.N. Palazotto, and R.A. Kemnitz. Modeling and simulation techniques used in high strain rate projectile impact. *Mathematics*, 9(3):274, 2021, doi: 10.3390/math9030274.

[21] M.R. Jensen and S. Grate. Procedure for fast ballistic vulnerability simulation of armored vehicles supported by finite element results and an extensive numerical sensitivity study of key parameters. *SAE Technical Paper* 2024-01-3901, 2021. doi: 10.4271/2024-01-3901.

[22] V. Mishra and V. Kukshal. Numerical analysis for estimating ballistic performance of armour material. *Materials Today: Proceedings*, 44(6):4731–4737, 2021. doi: 10.1016/j.matpr.2020.11.221.

[23] C. Chen, T. Liu, and Y. Cheng. Impact response of flowing-fluid filled square vessels. *Ocean Engineering*, 254:111405, 2022. doi: 10.1016/j.oceaneng.2022.111405.

[24] G. Chen, Y. Zhao, Y. Xue, K. Huang, and T. Zeng. Numerical investigation on performance of protective layer around large-scale chemical storage tank against impact by projectile. *Journal of Loss Prevention in the Process Industries*, 69:104351, 2021. doi: 10.1016/j.jlp.2020.104351.

[25] N. Lecysyn, A. Dandrieux, F. Heymes, L. Aprin, P. Slangen, L. Munier, C. Le Gallic, and G. Dusserre. Ballistic impact on an industrial tank: Study and modeling of consequences. *Journal of Hazardous Materials*, 172(2-3):587–594, 2009. doi: 10.1016/j.jhazmat.2009.07.086.

[26] M. Lee, R.G. Longoria, and D.E. Wilson. Ballistic waves in high-speed water entry. *Journal of Fluids and Structures*, 11(7):819–844, 1997. doi: 10.1006/jfls.1997.0103.

[27] Hutchinson. Osłona zbiorników SafeTank. Availavle: 7.07.2024. URL: https://www.hutchinson.com/pl/produkty/os%C5%82ona-zbiornik%C3%B3w-safetank.

[28] PN-EN 1523:2003. Okna, drzwi, żaluzje i zasłony. Kuloodporność. Metody badań. (in Polish).

[29] M. Roszak, D. Pyka, M. Bocian, N. Barsan, E. Dragašius, and K. Jamroziak. Multi-layer fabric composites combined with non-newtonian shear thickening in ballistic protection—hybrid numerical methods and ballistic tests. *Polymers*, 15(17):3584, 2023. doi: 10.3390/polym15173584.

[30] R. Scazzosi, A. Manes, and M. Giglio. An enhanced material model for the simulation of high-velocity impact on fiber-reinforced composites. *Procedia Structural Integrity*, 24:53–65, 2019. doi: 10.1016/J.PROSTR.2020.02.005.

[31] S.G. Nunes, R. Scazzosi, A. Manes, S.C. Amico, W.F. de Amorim Júnior, and M. Giglio. Influence of projectile and thickness on the ballistic behavior of aramid composites: Experimental and numerical study. *International Journal of Impact Engineering*, 132:103307, 2019. doi: 10.1016/J.IJIMPENG.2019.05.021.

[32] D. Pyka, A. Kurzawa, P. Żochowski, M. Bajkowski, M. Magier, R. Grygoruk, M. Roszak, K. Jamroziak, and M. Bocian. Experimental and numerical reserach on additional vehicles protection against explosives, *Archives of Civil and Mechanical Engineering*, 25:83, 2025. doi: 10.1007/s43452-025-01121-w.

[33] M.R. Vaziri, M. Salimi, and M. Mashayekhi. A new calibration method for ductile fracture models as chip separation criteria in machining. *Simulation Modelling Practice and Theory*, 18(9):1286–1296, 2010. doi: 10.1016/j.simpat.2010.05.003.

[34] G.-H. Lee, J.-W. Baek, J. Lim, S.-W. Kim, and S.-Y. Lee. Optimal prediction and validation of Johnson-Cook failure model for Al 6061 using genetic algorithm. *Journal of Mechanical Science and Technology*, 38:6085-6095, 2024. doi: 10.1007/s12206-024-1026-8.

[35] S. Akram, S.H.I. Jaffrey, M. Khan, M. Fahad, A. Mubashar, and L. Ali. Numerical and experimental investigation of Johnson-Cook material models for aluminum (Al 6061-T6) alloy using orthogonal machining approach. *Advances in Mechanical Engineering*, 10(9):1–14, 2018. doi: 10.1177/1687814018797794.